ACS OMEGA

Article

http://pubs.acs.org/journal/acsodf

Role of Surface Hydrophobicity of Dicationic Amphiphile-Stabilized Gold Nanoparticles on A549 Lung Cancer Cells

Thangavel Muthukumarasamyvel,[†] Ganapathy Rajendran,[‡] Devendrapandi Santhana Panneer,[†] Jayapalan Kasthuri,[§] Krishnan Kathiravan,[‡] and Nagappan Rajendiran*[,†]

[†]Department of Polymer Science and [‡]Department of Biotechnology, University of Madras, Guindy Campus, Chennai 600025, Tamil Nadu, India

[§]Department of Chemistry, Quaid-E-Millath Government College for Women (Autonomous), Chennai 600002, Tamil Nadu, India

Supporting Information

ABSTRACT: Herein, we report the surface functionality of dicationic cysteamine conjugated cholic acid (DCaC), dicationic cysteamine conjugated deoxycholic acid (DCaDC), and dicationic cysteamine conjugated lithocholic acid (DCaLC) templated gold nanoparticles (AuNPs) on mammalian cells. The haemocompatibility of the synthesized NPs was evaluated by in vitro hemolysis and erythrocyte sedimentation rate using human red blood cells (RBCs). In all of the systems, no toxicity was observed on human erythrocytes (RBCs) up to the concentration of 120 μg/mL. The anticancer activity of these dicationic amphiphile-stabilized AuNPs on A549 lung cancer cells was demonstrated by in vitro cell viability assay, intracellular reactive oxygen species estimation by DCFH-DA, apoptosis analysis using AO-EtBr fluorescence staining, DNA fragmentation analysis by agarose gel electrophoresis, and western blot analysis of caspase-3 expression. These results suggest that the cytotoxicity of AuNPs to A549 cells increase with the dose and hydrophobicity of amphiphiles and were found to be in the order: DCaLC-AuNPs > DCaDC-AuNPs > DCaC-AuNPs.

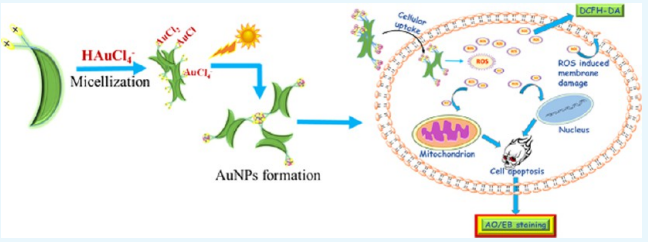

INTRODUCTION

In recent years, gold nanoparticles (AuNPs) have been used as promising key materials for biomedical applications such as cell labeling, imaging, biosensing, gene and drug delivery owing to their unique structure, tunable optical properties, chemical inertness, and biocompatibility.[1−3] Considering the biological perspective, efforts have been devoted to develop an environmentally benign synthetic approach using a clean, eco-friendly reducing and capping agent and an environmentally suitable solvent system for the preparation of AuNPs.[4,5] Recent studies have shown that the size, shape, surface charge, and functionality of NPs play a significant role in determining the intracellular uptake and localization of the NPs as well as their biological functions.[6,7] In particular, the surface charge of the nanomaterials plays a crucial role in determining the molecular interactions, cellular uptake, and cytotoxicity of NPs with biological systems.[8] In addition to charge, NP surface functionality has been involved in the process of cellular uptake and eliciting cellular responses.[9,10] For instance, Stellacci et al. have reported the effect of surface properties of NPs on the negatively charged cell membrane.[10b] Recently, the Rotello group have demonstrated the behavior of AuNPs with different hydrophobicities and the effect of surface functionality on hemolysis.[11,12] They observed linear hemolytic behavior with increasing hydrophobicity in the absence of serum media. The evaluation of different surface-charged AuNPs with cell lines was demonstrated in a dose-dependent manner.[13,14] These findings illustrated that the positively charged AuNPs were more internalized by cells than neutral or negatively charged NPs.

Cancer is a major terrible threat to public health and has the highest mortality rates worldwide. Conventionally practiced therapy with cytotoxic drugs fails to cure most cancer patients with advanced disease due to the presence or development of resistance to anticancer agents.[15,16] There is growing evidence that targeting multiple cell death pathways may be an advantageous strategy for the treatment of cancer.[17,18] Nanomaterials are expected to revolutionize cancer diagnosis and therapy.[19] Several studies have shown that AuNPs serve as carriers for biomolecules or drugs against some cancer cells.[20−23] In addition to this study, AuNPs can be envisioned as anticancer agents in their own right by generation of reactive oxygen species (ROS) in cells.[24] Zhao et al. have reported that AuNPs generated more intracellular ROS in lung cancer cells with low intracellular GSH.[25] Hahm et al. and Morgan et al. have reported that at higher concentrations, ROS often causes cellular damage and leads to cell death including apoptosis and necrosis.[26,27] Moreover, it is established that hydrophobicity plays an important role in the generation of ROS, DNA damage, and hence potential genotoxicity.[10a] Herein, we report haemocompatible and in vitro anticancer activity against A549 lung cancer cell lines using three bile acid-based amphiphile-

Received: March 24, 2017
Accepted: June 12, 2017
Published: July 25, 2017

DOI: 10.1021/acsomega.7b00353
ACS Omega 2017, 2, 3527−3538

templated AuNPs featuring dicationic head groups differing in degree of hydrophobicity. The effect of particle hydrophobicity on cancer cells was analyzed, and the results suggest that the highly hydrophobic nanoparticles possess high anticancer properties and induced caspase-3 mediated apoptosis by the generation of ROS.

RESULTS AND DISCUSSION

Synthesis of Dicationic Amphiphile-Stabilized AuNPs. The bile acid-based dicationic amphiphiles were prepared by adopting our previously reported method,[28] and the chemical structure is displayed in Scheme 1. The reaction was

Scheme 1. Chemical Structure of Dicationic Amphiphiles

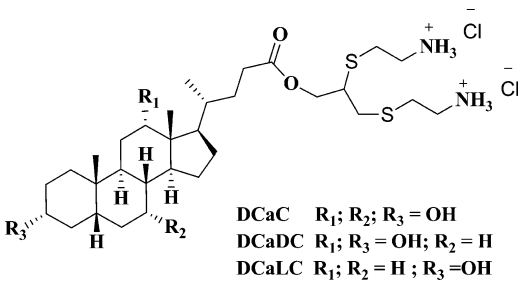

demonstrated by mixing 1×10^{-3} M of $HAuCl_4$ ions with optimized concentrations of dicationic cysteamine conjugated cholic acid (DCaC) (1×10^{-4} M), dicationic cysteamine conjugated deoxycholic acid (DCaDC) (2×10^{-4} M), and dicationic cysteamine conjugated lithocholic acid (DCaLC) (8.3×10^{-5} M) in aqueous medium at mid acidic pH ranging from 3.5 to 4.5. The reaction mixture was shaken well and then kept under bright sunlight irradiation. The formation of AuNPs was monitored by observing the change in solution color from light yellow to colorless and finally to pink. The reaction was completed within 90, 180, and 160 min for DCaC-, DCaDC-, and DCaLC-stabilized NPs, respectively. These dicationic amphiphiles stabilized AuNPs show characteristic surface plasmon resonance around 530 nm (Figure 1) with a stability of more than 6 months. The size and shape of the NPs were characterized by transmission electron microscopy (TEM) measurements showing that the particles are nearly spherical in shape with average sizes of 24 ± 2, 25 ± 3, and 22 ± 3 nm for DCaC-, DCaDC-, and DCaLC-stabilized NPs, respectively. Furthermore, the dynamic light scattering (DLS) studies provide the hydrodynamic radii of DCaC-, DCaDC-, and DCaLC-stabilized NPs and were measured to be 47.12, 44.43, and 45.58 nm, respectively (Figure 1d). The existence of positive charges on the NP surface was confirmed by zeta potential measurements and was found to be +20.30, +31.54, and +25.29 mV for DCaC-, DCaDC-, and DCaLC-stabilized AuNPs respectively (Figure 1e). The size, surface charge, and contact angle[28] measurements of synthesized NPs are compared in Table S1. The synthesized AuNPs were purified by high speed centrifuge (Lark innovative fine teknowledge, India) at 24 000 rpm maintained at 4 °C for 30 min to remove free amphiphiles. After centrifugation, AuNPs pellets were resuspended in deionized water and centrifuged thrice in the same manner to ensure complete removal of extraneous matter. Finally, the purified Au colloidal dispersion was collected, lyophilized, and stored for further characterization.[5b] The concentrations of the three dicationic amphiphile-stabilized AuNPs were calculated by adopting the previously reported protocol,[29] and the values were found to be 3.72, 3.30, and 4.82 nM for DCaC-, DCaDC-, and DCaLC-stabilized AuNPs, respectively.

Haemocompatibilty Studies. *Erythrocyte Sedimentation Rate (ESR).* ESR is the traditionally used standard clinical test to detect the sedimentation rate of erythrocytes (red blood cells (RBCs)). The sedimentation rate is influenced by three factors including the surface of the RBCs, plasma concentration, and size and shape of the RBCs. Under normal condition, the rouleaux formation of RBCs is low. Upon interaction with AuNPs, not much change in the ESR was observed indicating that the NPs do not affect the normal rouleaux formation (Figure 2). The sedimentation rates were measured over a period of 1 h and found to be 8, 10, and 12 mm for DCaC-AuNPs, DCaDC-AuNPs, and DCaLC-AuNPs, respectively. The obtained results were within the normal values of the Westergren method and show preliminary evidence to support its clinical utility.

In Vitro Haemotoxicity Analysis. The hemolysis assay is a procedure routinely used by hospital-based clinical and research laboratories specializing in complement-related studies.[30] Because the toxicity of NPs is highly dependent on its physicochemical and surface properties, it is essential to evaluate the blood compatibility of AuNPs for biomedical applications. The hemolytic assay results showed that all of the tested amphiphile-stabilized AuNPs exhibit concentration-dependent hemolysis with the very lowest activity (Figure 3). At the highest concentration (120 μg/mL), the hemolytic activities of DCaC-, DCaDC-, and DCaLC-stabilized AuNPs were found to be 1.90, 1.97, and 2.09%, respectively. According to reports, tested samples with less than 5% hemolytic activity could be considered haemocompatible.[31] In this study, these amphiphile-stabilized AuNPs had good haemocompatibility up to the concentration of 120 μg/mL. The light microscopy observations of RBCs treated with dicationic amphiphile-stabilized AuNPs further supports the results of haemocompatibility (Figure 4). As more than 90% of the erythrocytes retained their original oval shape without any aggregation, they could be used for future biological and biomedical applications.

In Vitro Anticancer Activity of Dicationic Amphiphile-Stabilized AuNPs against A549 Human Lung Cancer Cell Line. Cytotoxicity studies of NPs depend on particle size, shape, composition, surface charge, and hydrophobicity. Although correlation of cytotoxic effect and size of NPs has been studied extensively,[32−36] a limited number of reports are available for the effect of surface charge and hydrophobicity.[14,37,38] In this study, the anticancer activity of the synthesized AuNPs was investigated against A549 human lung cancer cells using the standard MTT cell assay method. The percentage of cell viability inhibition was calculated at different concentrations of DCaC-, DCaDC-, and DCaLC-stabilized AuNPs (20−120 μg/mL) for 24 h, and the obtained results are displayed in Figure 5. The results show that 3.71 and 24.26% inhibition of cell viability at 20 and 120 μg/mL, respectively, in DCaC-AuNPs. For DCaDC-AuNPs, the figures were 3.45% at 20 μg/mL and 43.77% at 120 μg/mL inhibition, respectively. In the case of DCaLC, the inhibition was found to be 4.43 and 46.89% at 20 and 120 μg/mL, respectively. Among these, the DCaLC system showed better inhibitory activity at both the lowest and highest concentrations. These results suggest that the increased hydrophobicity of amphiphiles with positively surface-charged NPs show more efficiency in perturbing the structure or partly digesting cell membranes and interacting with cellular materials

DOI: 10.1021/acsomega.7b00353
ACS Omega 2017, 2, 3527−3538

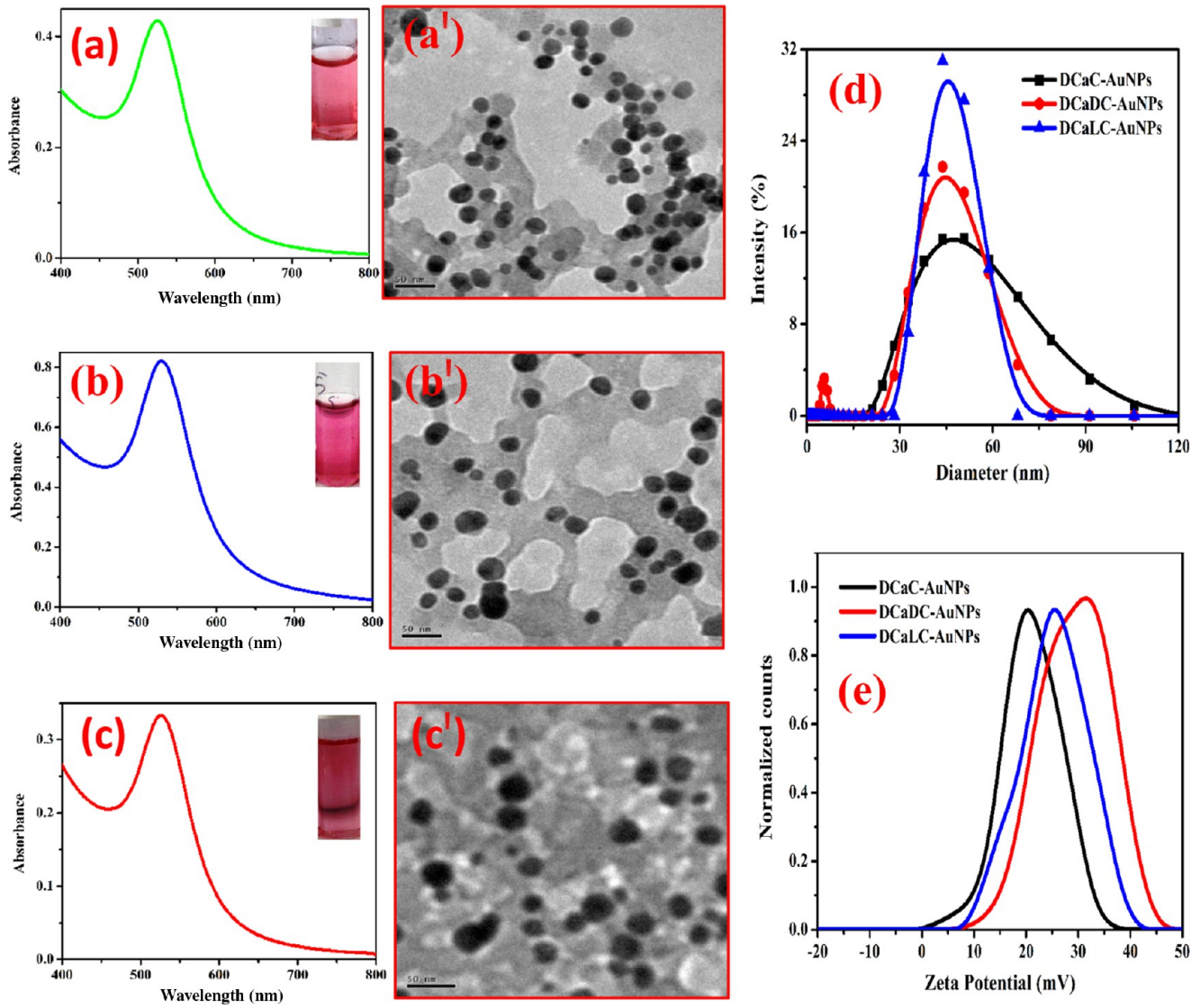

Figure 1. UV−visible absorption spectra and TEM images of AuNP solutions obtained by mixing $HAuCl_4$ (1×10^{-3} M) with DCaC (a, a′), DCaDC (b, b′), and DCaLC (c, c′) under sunlight exposure. Inset shows the photographs of the corresponding solutions. (d, e) DLS and zeta potential of AuNPs, respectively.

thereby suppressing cancer cell proliferation. Previous reports also show that hydrophobic coated NPs play a significant role in cell membrane damage than that of the uncoated NPs.[39] Rotello et al. demonstrated that increasing the hydrophobicity on the NP surface resulted in higher cytotoxicity with concomitant ROS production.[40] The results obtained from MTT assay were further supported by inverted microscopy analysis (Figure 6). The morphological evaluation of cells treated with DCaDC-AuNPs and DCaLC-AuNPs (120 μg/mL) for 24 h revealed a decrease in the proliferation activity, and the actual polygonal morphology of these cells show membrane damage. The salient morphological features of apoptosis such as distorted shape, membrane blebbing, and loss of cell membrane asymmetry, and cell shrinkages are indicated by yellow doted circles (Figure 6). This provides strong evidence that the cytotoxicity of AuNPs to A549 cells not only increased in a dose-dependent manner but also depends on the hydrophobicity of AuNPs. Hence, these AuNPs could be considered as a vector for drug delivery to treat cancer after detailed studies in the future.

Estimation of Intracellular ROS. ROS is a specific type of oxygen-containing reactive molecule, playing important roles in various cellular processes and is known to be essential for cell proliferation at basal levels. However at sufficiently high concentrations, ROS could become cytotoxic, often entailing cellular necrosis or apoptosis.[41,42] DCFH-DA is a non-fluorescent dye used to measure the intracellular ROS generation of cells. It can enter the plasma membrane passively, where it is converted to fluorescent DCFH by the action of peroxides in the presence of peroxidases.[43] To understand the mechanism of apoptosis induced by the amphiphile-stabilized AuNPs in A549 cells (Scheme 2), quantitative analysis of ROS was performed by spectrofluorometer (Figure 7). The generation of ROS level compared to that of control for DCaC-, DCaDC-, and DCaLC-stabilized AuNPs follows the increasing order of 1.25, 2.12, and 2.55 fold, respectively. The obtained results also clearly indicate that the apoptosis of A549 cells induced by the different AuNPs through ROS generation was facilitated by the increased hydrophobicity of the AuNPs.

DOI: 10.1021/acsomega.7b00353
ACS Omega 2017, 2, 3527−3538

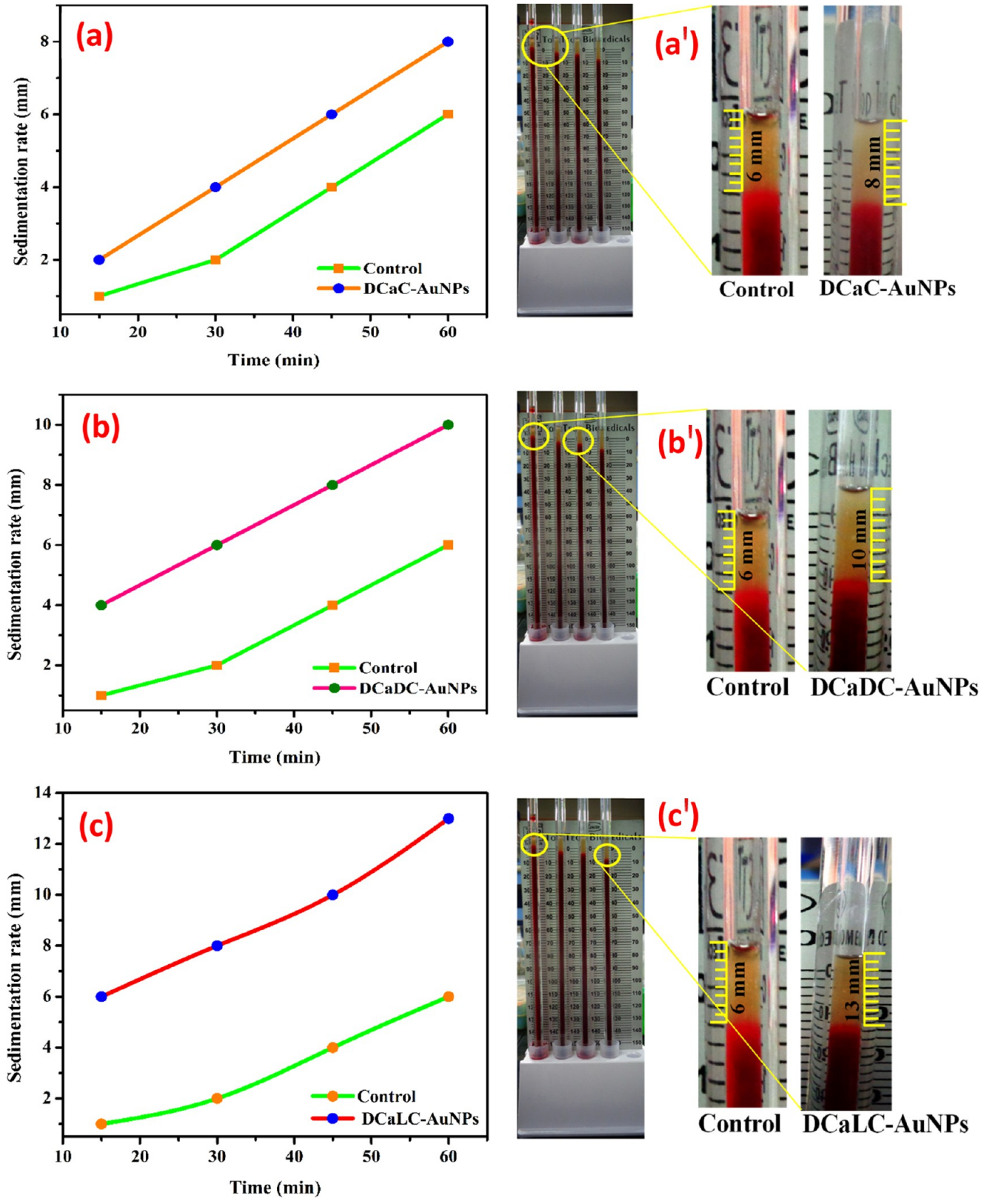

Figure 2. ESR of DCaC-AuNPs (a), DCaDC-AuNPs (b), and DCaLC-AuNPs (c) treated human RBC. (a′−c′) Sample-loaded Westergren tubes.

Fluorescence Microscopy Analysis of Cell Death. To determine the morphological changes of treated cells by the apoptotic effect of AuNPs, AO-EtBr staining was carried out. After the administration of 120 μg/mL of NPs for 24 h, the cells stained using AO-EtBr staining appeared green and yellow or red in color with associated apoptotic features such as apoptotic bodies and nuclear condensation. The florescence micrographs of untreated control cells exhibit normal nuclear architecture with uniform green fluorescence. After treatment with DCaC-AuNPs, early apoptotic cells with yellow or

DOI: 10.1021/acsomega.7b00353
ACS Omega 2017, 2, 3527−3538

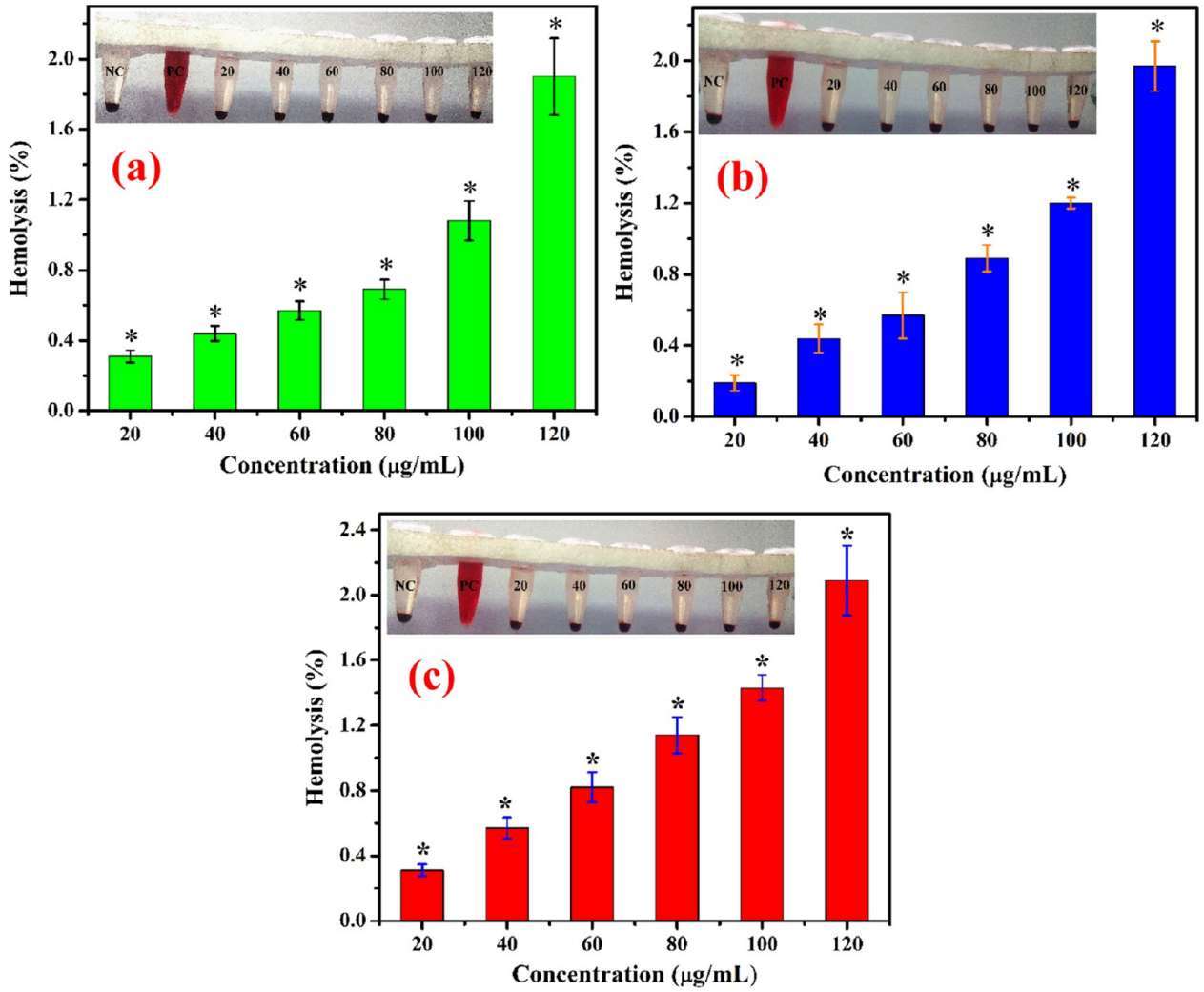

Figure 3. Hemolytic activity of dicationic amphiphile-stabilized AuNPs on human RBC at various concentrations ranging from 20 to 120 μg/mL (a) DCaC-AuNPs, (b) DCaDC-AuNPs, and (c) DCaLC-AuNPs. The inset shows the photographs of the corresponding solution. Here, (*) represents a significant difference ($p < 0.05$) compared to that of positive control.

yellowish green fluorescence were noted, as indicated by arrows (Figure 8b). This is also supported by the MTT assay performed on DCaC-AuNP treated A549 cells, which showed a high percentage of cell viability. However, in the cases of DCaDC- and DCaLC-stabilized AuNPs (Figure 8c,d), considerable cell death was observed, and it was clearly evidenced from the greenish yellow and yellow orange fluorescence of the dead cells. Our results corroborate a similar observation reported in previous studies showing that the hydrophobicity and surface charge of NPs can influence the capacity to produce ROS.[44] Recently, Rotello et al. have reported the role of surface functionality of cationic AuNPs on acute cytotoxicity, ROS generation, and DNA damage.[10] From the results obtained from this study and previous reports, it is clear that the surface functionality of NPs favors cytotoxicity through NP internalization. In particular, hydrophobicity of the NP surface is as important as surface charge in dictating cytotoxicity.

DNA Fragmentation. Because DNA shearing and fragmentation is considered to be the hallmark of apoptosis, the occurrence of apoptosis was determined by two factors, reduced and shrunken cells and DNA fragmentation.[45] Figure 9 shows the agarose gel electrophoresis of nuclear DNA from the control and dicationic amphiphile-templated AuNP treated A549 cells. It is observed that in lane 3, the isolated DNA from DCaC-treated cells shows no significant DNA damage. However, isolated DNA from DCaDC-AuNPs (lane 4) and DCaLC-AuNPs (lane 5) were sheared significantly. In particular, lane 5 shows well sheared and fragmented DNA. The results obtained from this study further supports the notion that the dicationic amphiphile-templated AuNPs induces apoptosis through increased hydrophobicity as compared with untreated cell DNA (lane 2).

Western Blot Assay. Previous studies have demonstrated that the caspase-3 cascade activation is responsible for several apoptotic mechanisms through induction of the cell cycle phase, genomic profile, and so on. Thus, it is obvious that DNA fragmentation and caspase-3 activation mediate the apoptotic process initiated either through the extrinsic or intrinsic pathway by the toxicants.[45,46] In the present study, the caspase-3 production in DCaC-, DCaDC-, and DCaLC-AuNPs induced in apoptotic cells was examined using Western blot analysis and densitometry showing that the magnitude of caspase-3 production in DCaC, DCaDC, and DCaLC increased one, two, and three fold, respectively (Figure 10).

DOI: 10.1021/acsomega.7b00353
ACS Omega 2017, 2, 3527−3538

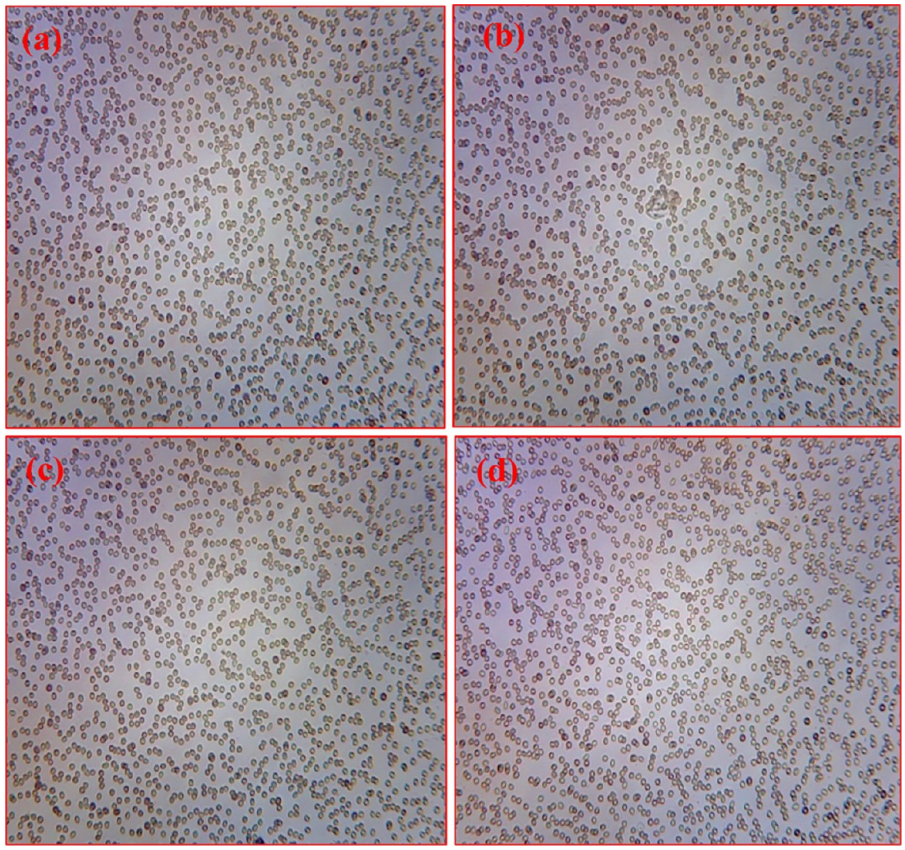

Figure 4. Photomicrographs of dicationic amphiphile-stabilized AuNP treated human RBC by light microscopy: (a) control RBC, (b) RBC treated with DCaC-AuNPs, (c) DCaDC-AuNPs, and (d) DCaLC-AuNPs at the highest concentration of 120 μg/mL.

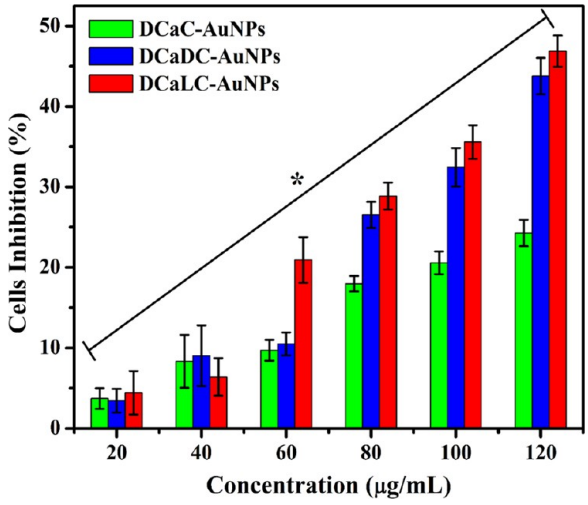

Figure 5. Cytotoxic effect of DCaC-, DCaDC-, and DCaLC-stabilized AuNPs on A549 lung cancer cells by MTT assay for 24 h at concentrations ranging from 20 to 120 μg/mL. Here, (*) represents a significant difference ($p < 0.05$) compared with that of control.

Statistical Methods. All of the data were analyzed using SPSS/10.0 software, and data were analyzed with one-way analysis of variance (ANOVA) followed by the post hoc Tukey test. The difference was considered statistically significant at $p \leq 0.05$. All experiments were carried out in triplicate.

CONCLUSIONS

In conclusion, we have demonstrated that the surface hydrophobicity of dicationic amphiphiles plays a prominent role in the intracellular uptake of AuNPs. The NPs showed good haemocompatibility up to the concentration of 120 μg/mL and anticancer activity against A549 human lung cancer cells, evaluated using the standard MTT assay. Among these, DCaLC-AuNPs showed better inhibitory activity at both the lowest and highest concentrations. The ROS generation in DCaLC-stabilized AuNPs showed a 2.55 fold increase when compared with that of control. The effect of particle hydrophobicity on cancer cells was analyzed, it was observed that the NPs with greater hydrophobicity possess high anticancer properties and induce caspase-3-mediated apoptosis by the generation of ROS. These results suggest that the degree of surface hydrophobicity of the synthesized NPs causes severe toxicity with respect to ROS generation. Hence, these AuNPs with good haemocompatibility and anticancer properties could be used effectively for cancer therapeutics in biomedical applications.

EXPERIMENTAL SECTION

Materials. Cholic acid (CA, 98%), DCA (98%), lithocholic acid (98%), fetal bovine serum (FBS), Antibiotic−Antimycotic from Gibco laboratory, 3-(4,5-dimethylthiazol-2-yl)-2,5-diphenyl tetrazolium bromide (MTT), dichlorofluorescin diacetate (DCFH-DA), acridine orange (AO), ethedium bromide (EtBr), CelLytic M, Triton X 100, and Trypan blue were purchased from Sigma-Aldrich, India. Also, 3,3-diaminobenzidine tetrahydrochloride (DAB), hydrogen peroxide, acrylamide, bisacryla-

DOI: 10.1021/acsomega.7b00353
ACS Omega 2017, 2, 3527−3538

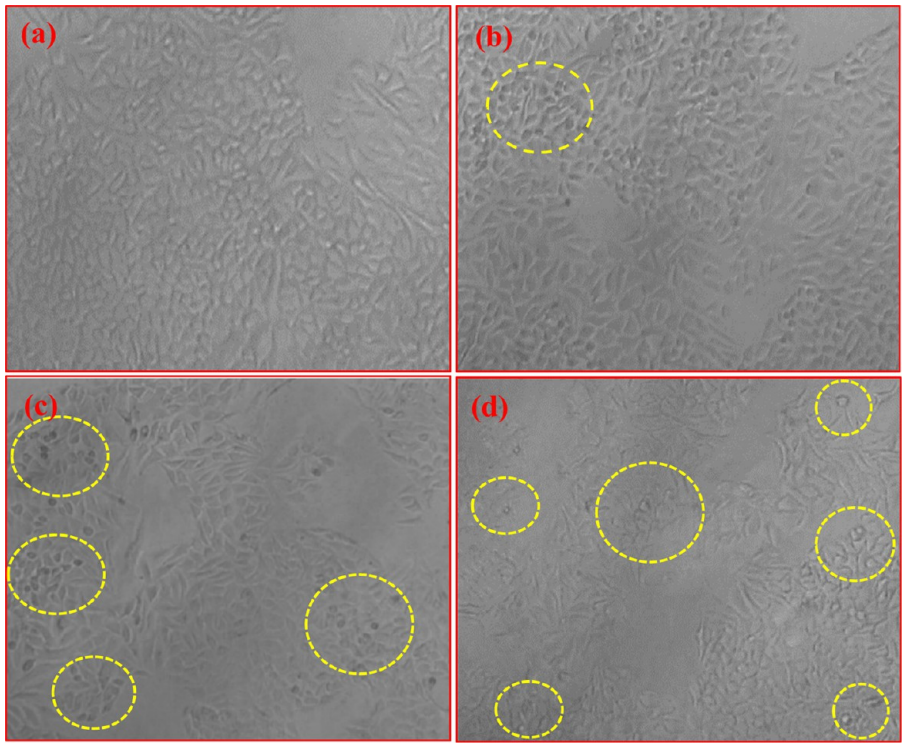

Figure 6. Morphological observation of A549 lung cancer cells: (a) control, (b) treated with DCaC-AuNPs, (c) DCaDC-AuNPs, and (d) DCaLC-AuNPs at the highest concentration of 120 μg/mL.

Scheme 2. Proposed Mechanism of ROS-Induced Cell Apoptosis

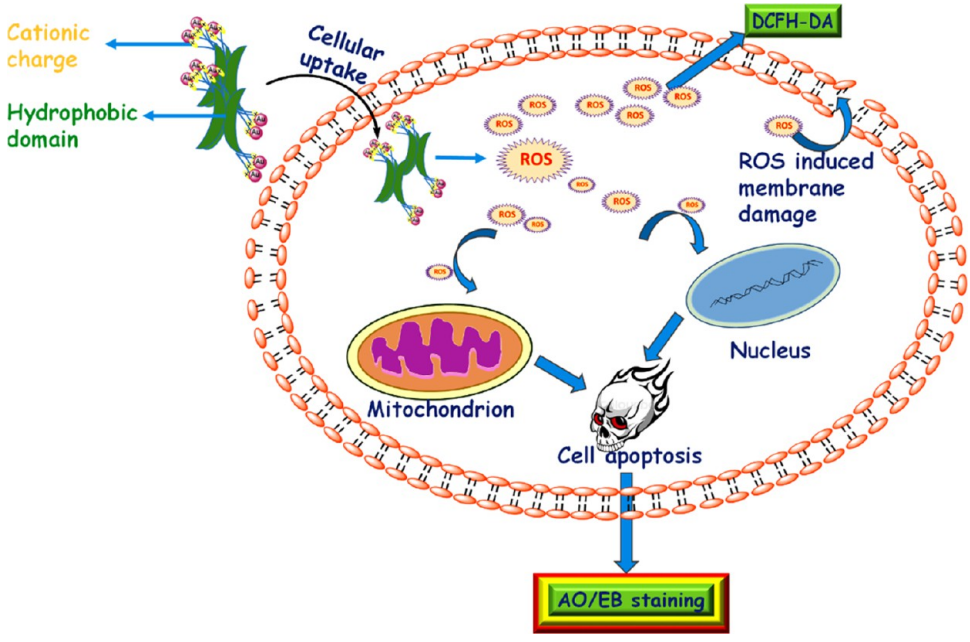

mide, sodium dodecyl sulfate (SDS), ammonium persulfate, tetramethylethylenediamine, glycine, Tris base, bromophenol blue, β-mercapto ethanol, bovine serum albumin (BSA), Tween 20, sodium acetate, phenol, chloroform, isoamyl alcohol, ethanol, and methanol were purchased from SRL Pvt. Ltd. India. Ham's F12K medium and trypsin phosphate versene glucose were purchased from Himedia laboratory, India. PVDF membrane was purchased from GE Healthcare, India. Primary antibody monoclonal (Rabbit) (β-actin (1:1000 dilution) and Caspase 3 (1:1000 dilution) were purchased from Cell Signaling Technology, HRP-conjugated antirabbit secondary antibody was purchased from Bangalore Genei, India. All materials and solvents were used as received from the suppliers with no further purification. The glass containers were washed with aqua-regia (HCl/HNO_3, 3:1, v/v) and then rinsed with double distilled water.

High-Resolution Transmission Electron Microscope (HR-TEM). HR-TEM images were recorded with a JEOL JEM 2100 equipped with a Gatan imaging filter. The HR-TEM analysis was conducted by placing a drop of the nanoparticle

DOI: 10.1021/acsomega.7b00353
ACS Omega 2017, 2, 3527−3538

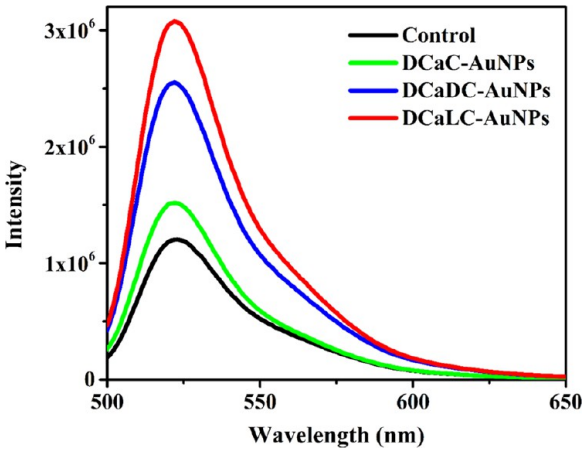

Figure 7. Dicationic amphiphile-stabilized AuNP induced ROS analysis by DCFH-DA in A549 lung cancer cells using spectrofluorometer at the highest concentration of 120 μg/mL.

solution on a carbon-coated copper grid and followed by solvent evaporation under ambient temperature. The average size of the nanoparticles was analyzed using imagej software.

DLS and Zeta Potential Measurements. The DLS and zeta potential of amphiphile-stabilized AuNPs were measured in aqueous medium using a Malvern zetasizer nano ZS system.

Contact Angle Measurements. For contact angle measurements, a good-quality glass plate was selected and diced to specific sizes (25 mm × 25 mm). The glass slide was cleaned using piranha solution (3:1 mixture of H_2SO_4 and H_2O_2) and subsequently dried using nitrogen gas. The same protocol was repeated for each surfactant, and all of the surfactant solutions were prepared freshly before the experiments. Contact angle measurements (θ) were carried out via the dynamic sessile drop method using a surface tensiometer, Data Physics (DCAT 11EC), equipped with a Hamilton Syringe. Liquid droplets (4 μL) were used in each measurement.

Blood Sample Collection. A healthy donor was selected for blood sample collection. Before blood collection, the donor was screened for basic eligibility for blood donation using factors like anemia, age, weight, drunken, state, drugs, surgery, and so on. The blood sample was collected from the vein and gently mixed with the appropriate volume of anticoagulant and stored at 4 °C for further analysis.

Estimation of ESR. ESR measures the rate of sedimentation of RBCs under standard conditions, wherein the drastic changes in sedimentation rate are indicative of disease progression. According to the Westerngren method, the normal value should be 15 mm/h.[47] The amphiphile-stabilized AuNPs were separately added to the collected blood sample at a concentration of 120 μg/mL, then the blood samples were loaded into the Westergren tubes upto the mark around zero, and the untreated blood sample was considered as a control. All of the tubes were vertically allowed to stand for 1 h without any disturbance. The ESR rate was measured every 15 min, and the obtained results were recorded.

In Vitro Hemolytic (Erythrocyte) Toxicity Analysis. The in vitro hemolytic toxicity of DCaC-, DCaDC-, and DCaLC-stabilized AuNPs were studied by measuring the percentage of hemoglobin released from the human erythrocytes by adopting the previously reported protocol with a slight modification.[48] Collected blood samples were centrifuged at 1500 rpm for 15 min in a cooling centrifuge. The supernatant plasma and buffy coat were carefully removed, and the pellet erythrocytes were gently washed three times with a sterile saline solution. Erythrocyte suspension (5%) was prepared with a saline solution, and 1 mL of the suspension was added to each tube containing 20, 40, 60, 80, 100, and 120 μg of the DCaC-, DCaDC-, and DCaLC-stabilized AuNPs. Negative and positive controls were also prepared by 1 mL of cell suspension (blank) and the cell suspension containing Triton X-100 (1%), respectively. All of the tubes were incubated at 37 °C for 1 h and were centrifuged at 2000 rpm for 10 min. Then, the supernatant was collected in separate tubes to measure the optical density values at 540 nm against the blank by using an UV−visible spectrophotometer. The percentage of hemolysis was calculated using the following formula.

$$\text{hemolysis (\%)} = \left[\frac{\text{OD}^{\text{sample}} - \text{OD}^{\text{blank}}}{\text{OD}^{\text{Triton X}} - \text{OD}^{\text{blank}}}\right] \times 100$$

The calculated percentages of hemolysis for all of the samples were compared to those of the ASTM standard,[49] that is, highly haemocompatible (<5% hemolysis), haemocompatible (within 10% hemolysis), and nonhaemocompatible (>20% hemolysis). Erythrocyte morphology was analyzed at the highest concentration (120 μg/mL) of the NP-interacted cell suspension. Cells were prepared at a ratio of 1:9 of cells and saline solution and examined under the low-power objective (10×) of the optical microscope (Olympus CH20i) with the system-attached Celestron camera (2 MP).

Culture of A549 Lung Cancer Cell Line. The human lung cancer cell line, A549, was procured from the National Center for Cell Science, Pune, India, and the cells were maintained in Ham's F12 K medium. The media was supplemented with 10% (v/v) heat-inactivated FBS, 100 μg/mL streptomycin, 100 units/mL penicillin, and 50 μg/mL amphotericin B. The cells were cultured in a T25 flask with 3 mL of medium and kept in an incubator containing 5% CO_2 at 37 °C under a humidified atmosphere. After attaining confluence (about 75%), these cells were subcultured once in 3 days and also observed for multiplication patterns and contamination under an inverted microscope (Motic AE31, Hong Kong). The cells in the exponential growth phase were used for all of the experiments.

Cell Counting. The cells were trypsinized and neutralized with complete medium. The trypan blue mixed cell suspension (1:1 ratio) was loaded in a haemocytometer, and the cells were counted with the help of a low-power objective (10×) in an optical microscope. The total number of cells per milliliter (mL) was calculated using the following formula.

$$(\text{no of cells counted/no of square counted}) \times (\text{dilution factor}) \times (10000)$$

Anticancer Activity of AuNPs against A549 Human Lung Cancer Cell Line. Anticancer activity of dicationic amphiphile-stabilized AuNPs against the lung cancer cell line was analyzed using the standard MTT(3-(4,5-dimethylthiazol-2-yl)-2,5-diphenyl tetrazolium bromide) assay, in which MTT was cleaved by mitochondrial dehydrogenase enzymes of viable cells and yielded purple-colored formazan crystals, which were solubilized using dimethyl sulfoxide (DMSO).[50] A549 cells were seeded at a concentration of 1×10^4 cells in each well of a 96-well tissue culture plate and incubated for 24 h at 37 °C in a 5% CO_2 incubator. The cell culture medium was replaced from

DOI: 10.1021/acsomega.7b00353
ACS Omega 2017, 2, 3527−3538

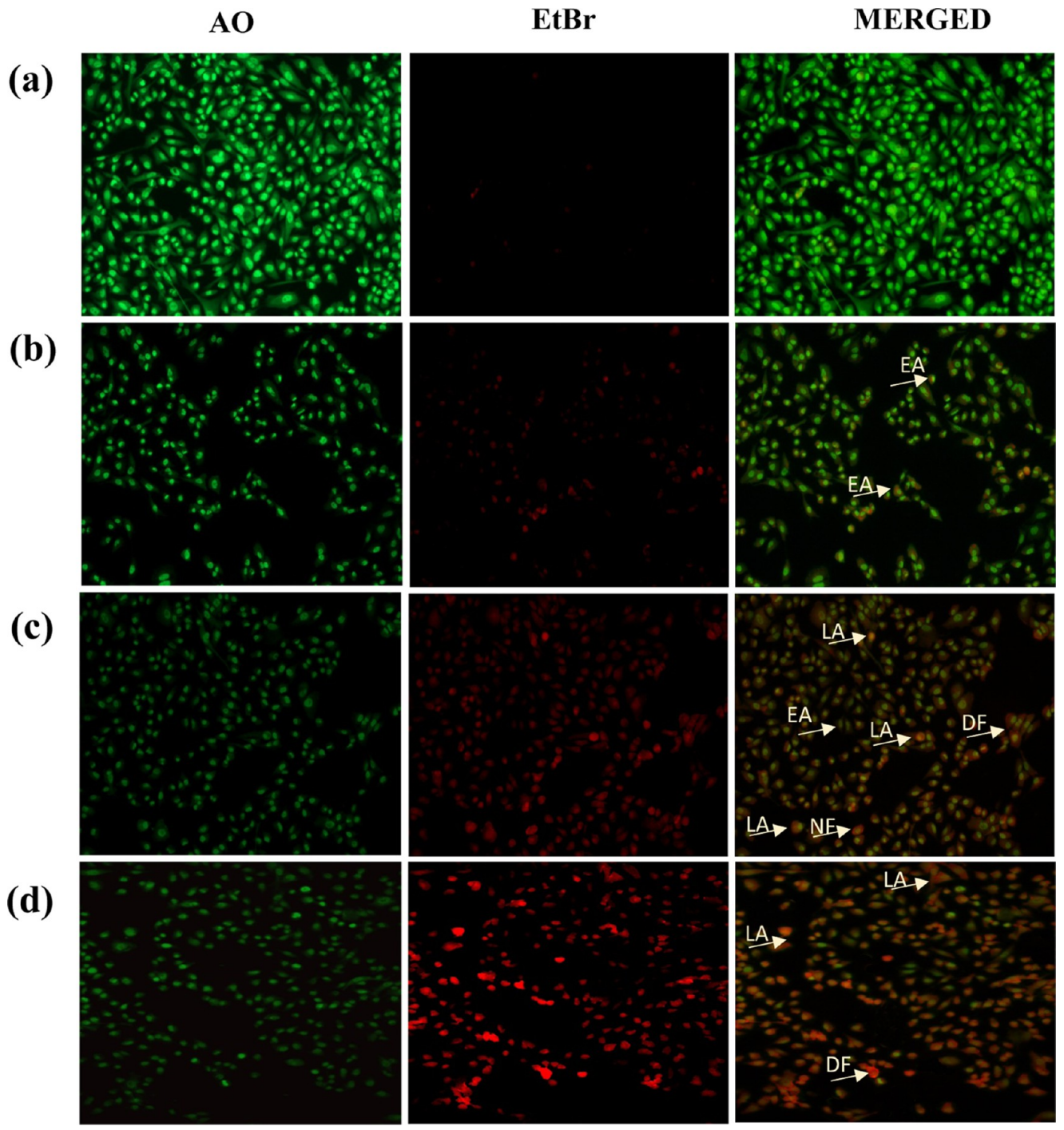

Figure 8. Fluorescence microscopy images of AO-EtBr staining for apoptosis in A549 cells: (a) control, (b) treated with DCaC-AuNPs, (c) DCaDC-AuNPs, and (d) DCaLC-AuNPs at the highest concentration of 120 μg/mL. (EA: early apoptosis; LA: late apoptosis; DF: DNA fragmentation).

each well by adding 100 μL of fresh medium. Different concentrations of DCaC-, DCaDC-, and DCaLC-stabilized AuNPs (20, 40, 60, 80, 100, and 120 μg/mL) were added into the respective wells, and the cells without NPs were considered as a control. The cells were incubated for 24 h in a 5% CO_2 incubator at 37 °C. MTT solution was freshly prepared (5 mg/mL PBS), and 10 μL was added into each well including control and incubated for 3 h under the above-said conditions. After that, the supernatant was carefully removed, and 100 μL of DMSO was added to dissolve the formazan crystals. Cytotoxicity was measured by recording the absorbance of the formed formazan purple color in an ELIZA reader (BIO-TEK, Powerwave-XS) at 570 nm. Cell viability (%) and cell inhibition (%) were calculated by using the following formula

$$\text{cell viability (\%)} = \left[\frac{\text{absorbance of sample}}{\text{absorbance of control}}\right] \times 100$$

$$\text{cell inhibition (IR)\%} = 100 - \text{cell viability (\%)}$$

Cell morphology of control and NP treated cells were analyzed using an inverted micrcoscope (Motic AE31, Hong Kong).

DOI: 10.1021/acsomega.7b00353
ACS Omega 2017, 2, 3527−3538

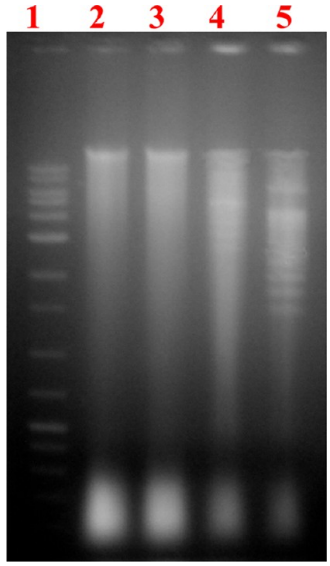

Figure 9. DNA fragmentation analysis using agarose gel electrophoresis. Lane 1: 10 Kb DNA ladder; lane 2: control DNA; lane 3: DCaC-treated cell DNA; lane 4: DCaDC-treated cell DNA; lane 5: DCaLC-treated cell DNA.

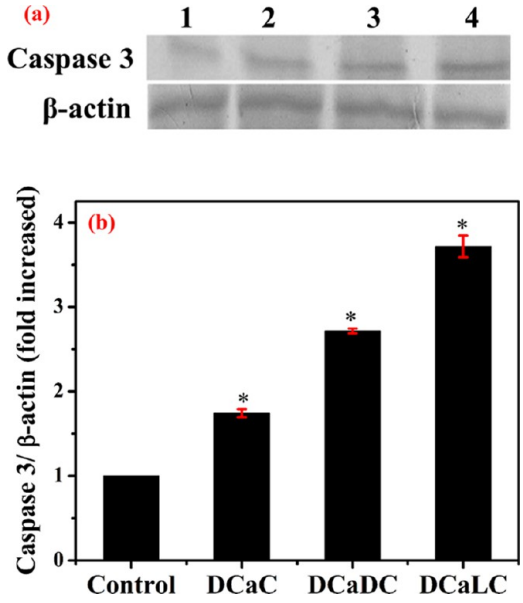

Figure 10. Western blot analysis of caspase 3 and β-actin of A549 cells (a): control (1); treated with DCaC-AuNPs (2); DCaDC-AuNPs (3); DCaLC-AuNPs (4). (b) Densitometry graph of the corresponding Western blot analysis of caspase 3. Here, (*) represents a significant difference ($p < 0.05$) compared to control.

AO-EtBr Staining. AO-EtBr is used to stain apoptotic cells. AO is permeable through the intact cell membrane and stained both live and dead cells, EtBr can pass only through the damaged cell membrane (lost membrane integrity). Apoptosis analysis was followed by adopting the previously reported protocol with a slight modification.[51] The cells were seeded in a six-well plate on a sterile cover slip at a concentration of 1×10^5 cells with 3 mL of Ham's F12K complete medium, and the cells were incubated in a 37 °C, 5% CO_2 incubator. After the attainment of >80% confluence, the cells were treated with 120 μg/mL of DCaC-, DCaDC-, and DCaLC-stabilized AuNPs, and the untreated cells were considered as control. These cells were allowed to incubate for 24 h and fixed on a cover slip and stained with AO-EtBr. The coverslip containing stained cells were placed on a clean glass slide at an inverted position and examined by a fluorescence microscope (Nikon ECLIPSE 80i) using fluorescein filter (450−490 nm).

Estimation of ROS by DCFH-DA. The intracellular ROS generation of cells can be investigated using the dichlorofluorescein-diacetate (DCFH-DA) as a well-established compound to detect intracellularly produced H_2O_2. Estimation of ROS by DCFH-DA is followed by adopting the previously reported protocol with a slight modification.[52] The cells (1×10^5) were seeded in a six-well plate and incubated in a 5% CO_2 incubator maintained at 37 °C. After confluence, the cells were treated with DCaC-, DCaDC-, and DCaLC-stabilized AuNPs at a concentration of 120 μg/mL, and untreated cells were considered as control. After 24 h incubation, the medium was removed, and the cells were stained with DCFH-DA (20 μm) for 20 min at 37 °C and subsequently washed with PBS and collected in a sterile centrifuge tube. The ROS was analyzed from each sample using a Fluoromax 4 spectrofluorometer (Horiba Jobin Yvon).

DNA Fragmentation Assay. DNA fragmentation assay was performed by adopting the previously reported protocol with a slight modification.[45] Briefly, 1×10^6 cells were seeded in a T75 flask with Ham F-12 kaighn's modification medium containing 10% FBS and kept in an incubator for 24 h in 5% CO_2 at 37 °C. After attaining confluence (about 80%), the cells were treated with a 120 μg/mL concentration of DCaC-, DCaDC-, and DCaLC-AuNPs for 24 h under the above-said conditions, and the cells without NPs were considered as a control. After 24 h, the cells were trypsinized and washed twice with PBS buffer (pH 7.4). The genomic DNA was isolated from treated and control cells. DNA (20 μg) was electrophoresed in 1.2% agrose gel containing EtBr in a gel tank with TAE buffer (pH 8) for 45 min at 100 V, and the gel was analyzed under the UV transilluminator.

Western Blot Analysis. The protein was isolated from the control and AuNP treated cells using cell lysis buffer and quantified. Protein (40 μg) was mixed with an equal volume of 1× SDS sample buffer (0.2 M Tris−HCl buffer, 10% glycerol, 2% SDS, 0.02% β-mercaptoethanol) and boiled for 10 min in a water bath. After cooling, the samples were loaded in SDS polyacrylamide gel electrophoresis (SDS PAGE) containing 5% stacking gel and 10% resolved gel. The resolved gel protein was transferred to the poly(vinylidene difluoride) (PVDF) membrane by electrophoresis. The membrane was blocked with PBS containing 0.1% Tween 20 and 5% BSA at RT and then probed with primary antibody β-actin (1:500 dilution), Caspase 3 (1:500 dilution), and incubated overnight at 4 °C. The membrane was washed with PBST (thrice), subsequently the HRP conjugated secondary antibody (1:1000 dilution) was added and incubated for 1 h at RT. After that, it was washed with PBS, and the protein antibody complexes were visualized using DAB as a chromogenic substrate. Relative protein levels normalized to β-actin were quantified using Image-J software (National Institutes of Health, Bethesda, MD).

■ ASSOCIATED CONTENT

Supporting Information

The Supporting Information is available free of charge on the ACS Publications website at DOI: 10.1021/acsomega.7b00353.

DOI: 10.1021/acsomega.7b00353
ACS Omega 2017, 2, 3527−3538

Comparison table of size and surface properties of AuNPs (PDF)

AUTHOR INFORMATION

Corresponding Author

*E-mail: nrajendiar@yahoo.com.

ORCID

Thangavel Muthukumarasamyvel: 0000-0002-5582-3480

Nagappan Rajendiran: 0000-0002-8903-5132

Notes

The authors declare no competing financial interest.

ACKNOWLEDGMENTS

The authors thank the Department of Science and Technology (DST), Government of India, for awarding the Inspire fellowship. Dr. N.R. thanks DST-EMEQ (No. SB/EMEQ-133/2013) for financial support. The National Center for Nanoscience and Nanotechnology, University of Madras, is thanked for the TEM analysis. We thank Dr. D. Mohan, Department of Chemical Engineering, Anna University, for providing the contact angle instrument facility.

REFERENCES

(1) Burda, C.; Chen, X.; Narayanan, R.; El-Sayed, M. A. Chemistry and Properties of Nanocrystals of Different Shapes. *Chem. Rev.* **2005**, *4*, 1025−1102.

(2) Hirsch, L. R.; Stafford, R. J.; Bankson, J. A.; Sershen, S. R.; Rivera, B.; Rrice, R. E.; Hazle, J. D.; Halas, N. J.; West, J. L. Nanoshell-Mediated Near-Infrared Thermal Therapy of Tumors Under Magnetic Resonance Guidance. *Proc. Natl. Acad. Sci. U.S.A.* **2003**, *100*, 13549−13554.

(3) Chandirasekar, S.; Dharanivasan, G.; Kasthuri, J.; Kathiravan, K.; Rajendiran, N. Facile Synthesis of Bile Salt Encapsulated Gold Nanoparticles and Its Use in Colorimetric Detection of DNA. *J. Phys. Chem. C* **2011**, *115*, 15266−15273.

(4) Annadhasan, M.; Muthukumarasamyvel, T.; Sankar Babu, V. R.; Rajendiran, N. Green Synthesized Silver and Gold Nanoparticles for Colorimetric Detection of Hg2+, Pb2+, and Mn2+ in Aqueous Medium. *ACS Sustainable Chem. Eng.* **2014**, *2*, 887−896.

(5) (a) Cho, E. C.; Au, L.; Zhang, Q.; Xia, Y. N. The Effects of Size, Shape, and Surface Functional Group of Gold Nanostructures on Their Adsorption and Internalization by Cells. *Small* **2010**, *6*, 517−522. (b) Dinesh, D.; Sunil, J.; Kiran, J. Nepenthes Khasiana Mediated Synthesis of Stabilized Gold Nanoparticles: Characterization and Biocompatibility Studies. *J. Photochem. Photobiol., B* **2016**, *154*, 108−117.

(6) Cho, E. C.; Zhang, Q.; Xia, Y. N. The Effect of Sedimentation and Diffusion on Cellular Uptake of Gold Nanoparticles. *Nat. Nanotechnol.* **2011**, *6*, 385−391.

(7) Carney, R. P.; Carney, T. M.; Mueller, M.; Stellacci, F. Dynamic Cellular Uptake of Mixed-Monolayer Protected Nanoparticles. *Biointerphases* **2012**, *7*, No. 17.

(8) Fröhlich, E. The Role of Surface Charge in Cellular Uptake and Cytotoxicity of Medical Nanoparticles. *Int. J. Nanomed.* **2012**, *7*, 5577−5591.

(9) (a) Yang, H.; Fung, S. Y.; Liu, M. Y. Programming The Cellular Uptake of Physiologically Stable Peptide−Gold Nanoparticle Hybrids With Single Amino Acids. *Angew. Chem., Int. Ed.* **2011**, *50*, 9643−9646. (b) Oh, E.; Delehanty, J. B.; Sapsford, K. E.; Susumu, K.; Goswami, R.; Blanco-Canosa, J. B.; Dawson, P. E.; Granek, J.; Shoff, M.; Zhang, Q.; Goering, P. L.; Huston, A.; Medintz, I. L. Cellular Uptake and Fate of Pegylated Gold Nanoparticles is Dependent on Both Cell-Penetration Peptides and Particle Size. *ACS Nano* **2011**, *5*, 6434−6448.

(10) (a) Chompoosor, A.; Saha, K.; Ghosh, P. S.; Macarthy, D. J.; Miranda, O. R.; Zhu, Z. J.; Arcaro, K. F.; Rotello, V. M. The Role of Surface Functionality on Acute Cytotoxicity, ROS Generation and DNA Damage by Cationic Gold Nanoparticles. *Small* **2010**, *6*, 2246−2249. (b) Verma, A.; Stellacci, F. Effect of Surface Properties on Nanoparticle-Cell Interactions. *Small* **2010**, *6*, 12−21. (c) Saha, K.; Bajaj, A.; Duncan, B.; Rotello, V. M. Beauty Is Skin Deep: A Surface Monolayer Perspective on Nanoparticle Interactions With Cells and Bio-Macromolecules. *Small* **2011**, *7*, 1903−1918.

(11) Saha, K.; Moyano, D. F.; Rotello, V. M. Protein Coronas Suppress the Hemolytic Activity of Hydrophilic and Hydrophobic nanoparticles. *Mater. Horiz.* **2014**, *1*, 102−105.

(12) Saha, K.; Kim, S. T.; Yan, B.; Miranda, O. R.; Alfonso, F. S.; Shlosman, D.; Rotello, V. M. Surface Functionality of Nanoparticles Determines Cellular Uptake Mechanisms in Mammalian Cells. *Small* **2013**, *9*, 300−305.

(13) Schaeublin, N. M.; Braydich-Stolle, L. K.; Schrand, A. M.; Miller, J. M.; Hutchison, J.; Schlager, J. J.; Hussain, S. M. Surface Charge of Gold Nanoparticles Mediates Mechanism of Toxicity. *Nanoscale* **2011**, *3*, 410−420.

(14) Arvizo, R. R.; Miranda, O. R.; Thompson, M. A.; Pabelick, C. M.; Bhattacharya, R.; Robertson, J. D.; Rotello, V. M.; Prakash, Y. S.; Mukherjee, P. Effect of Nanoparticle Surface Charge at the Plasma Membrane and Beyond. *Nano Lett.* **2010**, *10*, 2543−2548.

(15) Giaccone, G.; Pinedo, H. M. Drug Resistance. *Oncologist* **1996**, *1*, 82−87.

(16) Holohan, C.; Van Schaeybroeck, S.; Longley, D. B.; Johnston, P. G. Cancer Drug Resistance: An Evolving Paradigm. *Nat. Rev. Cancer* **2013**, *13*, 714−726.

(17) Xun, H.; Yanyan, X. Bypassing Cancer Drug Resistance by Activating Multiple Death Pathways - A Proposal from The Study of Circumventing Cancer Drug Resistance by Induction of Necroptosis. *Cancer Lett.* **2008**, *259*, 127−137.

(18) Speirs, C. K.; Hwang, M.; Kim, S.; Li, W.; Chang, S.; Varki, V.; Mitchell, L.; Schleicher, S.; Lu, B. Harnessing The Cell Death Pathway for Targeted Cancer Treatment. *Am. J. Cancer Res.* **2011**, *1*, 43−61.

(19) Rosarin, F. S.; Arulmozhi, V.; Nagarajan, S.; Mirunalini, S. Antiproliferative Effect of Silver Nanoparticles Synthesized Using Amla on Hep2 Cell Line. *Asian Pac. J. Trop. Med.* **2012**, *1*, 1−10.

(20) Akrami, M.; Balalaie, S.; Hosseinkhani, S.; Alipour, M.; Salehi, F.; Bahador, A.; Haririan, I. Tuning The Anticancer Activity of A Novel Pro-Apoptotic Peptide Using Gold Nanoparticle Platforms. *Sci. Rep.* **2016**, *6*, No. 31030.

(21) Kim, D.; Jeong, Y. Y.; Jon, S. A Drug-Loaded Aptamer-Gold Nanoparticle Bioconjugate for Combined CT Imaging and Therapy of Prostate Cancer. *ACS Nano* **2010**, *4*, 3689−3696.

(22) Patra, C. R.; Bhattacharya, R.; Mukherjee, P. Fabrication and Functional Characterization of Gold Nano Conjugates for Potential Application in Ovarian Cancer. *J. Mater. Chem.* **2010**, *20*, 547−554.

(23) Glazer, E. S.; Massey, K. L.; Zhu, C.; Curley, S. A. Pancreatic Carcinoma Cells are Susceptible to Noninvasive Radio Frequency Fields After Treatment With Targeted Gold Nanoparticles. *Surgery* **2010**, *148*, 319−324.

(24) Jain, S.; Hirst, D. G.; O'Sullivan, J. M. Gold Nanoparticles As Novel Agents for Cancer Therapy. *Br. J. Radiol.* **2012**, *85*, 101−113.

(25) Zhao, Y.; Gu, X.; Ma, H.; He, X.; Liu, M.; Ding, Y. Association of Glutathione Level and Cytotoxicity of Gold Nanoparticles in Lung Cancer Cells. *J. Phys. Chem. C* **2011**, *115*, 12797−12802.

(26) Hahm, E. R.; Moura, M. B.; Kelley, E. E.; Van, H. B.; Shiva, S.; Singh, S. V. Withaferin A-Induced Apoptosis in Human Breast Cancer Cells is Mediated by Reactive Oxygen Species. *PLoS One* **2011**, *6*, No. e23354.

(27) Morgan, M. J.; Liu, Z. G. Reactive Oxygen Species in TNFalpha-Induced Signaling and Cell Death. *Mol. Cells* **2010**, *30*, 1−12.

(28) Muthukumarasamyvel, T.; Baskar, R.; Chandirasekar, S.; Umamaheswari, K.; Rajendiran, N. Hierarchical Self-assembly of Bile acid-Derived Dicationic Amphiphiles and Their Toxicity Assessment on Microbial and Mammalian Systems. *ACS Appl. Mater. Interfaces* **2016**, *8*, 25111−25126.

DOI: 10.1021/acsomega.7b00353
ACS Omega 2017, 2, 3527−3538

(29) (a) Johnston, R. L. *Atomic and Molecular Clusters*; Taylor & Francis: London, 2002. (b) Lewis, D. J.; Day, T. M.; MacPherson, J. V.; Pikramenou, Z. Luminescent Nanobeads: Attachment of Surface Reactive Eu(III) Complexes to Gold Nanoparticles. *Chem. Commun.* **2006**, *13*, 1433−1435.
(30) Pham, C. T. N.; Thomas, D. G.; Beiser, J.; Mitchell, L. M.; Huang, J. L.; Senpan, A.; Hu, G.; Gordon, M.; Baker, N. A.; Pan, D.; Lanza, G. M.; Hourcade, D. E. Application of a Hemolysis Assay for Analysis of Complement Activation by Perfluorocarbon Nanoparticles. *Nanomedicine* **2014**, *10*, 651−660.
(31) Chandra, V. S.; Baskar, G.; Suganthi, R. V.; Elayaraja, K.; Joshy, M. I. A.; Beaula, W. S.; Mythili, R.; Venkatraman, G.; Kalkura, S. N. Blood Compatibility of Iron-Doped Nanosize Hydroxyapatite and Its Drug Release. *ACS Appl. Mater. Interfaces* **2012**, *4*, 1200−1210.
(32) Malugin, A.; Ghandehari, H. Cellular Uptake and Toxicity of Gold Nanoparticles in Prostate Cancer Cells: A Comparative Study of Rods and Spheres. *J. Appl. Toxicol.* **2010**, *30*, 212−217.
(33) Shang, L.; Nienhaus, K.; Nienhaus, G. U. Engineered Nanoparticles Interacting with Cells: Size Matters. *J. Nanobiotechnol.* **2014**, *12*, No. 5.
(34) Chithrani, B. D.; Ghazani, A. A.; Chan, W. C. W. Determining the Size and Shape Dependence of Gold Nanoparticle Uptake into Mammalian Cells. *Nano Lett.* **2006**, *6*, 662−668.
(35) Canton, I.; Battaglia, G. Endocytosis at The Nanoscale. *Chem. Soc. Rev.* **2012**, *41*, 2718−2739.
(36) Huang, K.; Ma, H.; Liu, J.; Huo, S.; Kumar, A.; Wei, T.; Zhang, X.; Jin, S.; Gan, Y.; Wang, P. C.; et al. Size-Dependent Localization and Penetration of Ultrasmall Gold Nanoparticles in Cancer cells, Multicellular Spheroids, and Tumors in vivo. *ACS Nano* **2012**, *6*, 4483−4493.
(37) Goodman, C. M.; Mccusker, C. D.; Yilmaz, T.; Rotello, V. M. Toxicity of Gold Nanoparticles Functionalized with Cationic and Anionic Side Chains. *Bioconjugate Chem.* **2004**, *15*, 897−900.
(38) Moyano, D. F.; Goldsmith, M.; Solfiell, D. J.; Landesman-Milo, D.; Miranda, O. R.; Peer, D.; Rotello, V. M. Nanoparticle Hydrophobicity Dictates Immune Response. *J. Am. Chem. Soc.* **2012**, *134*, 3965−3967.
(39) Yin, H.; Too, H. P.; Chow, G. M. The Effects of Particle Size and Surface Coating on The Cytotoxicity of Nickel Ferrite. *Biomaterials* **2005**, *26*, 5818−5826.
(40) Kim, S. T.; Saha, K.; Kim, C.; Rotello, V. M. The Role of Surface Functionality in Determining Nanoparticle Cytotoxicity. *Acc. Chem. Res.* **2013**, *46*, 681−691.
(41) Matés, J. M.; Segura, J.; Alonso, F.; Marquez, J. Intracellular Redox Status and Oxidative Stress: Implications for Cell Proliferation, Apoptosis, and Carcinogenesis. *Arch. Toxicol.* **2008**, *82*, 273−299.
(42) Minai, L.; Hayon, D. Y.; Yelin, D. High Levels of Reactive Oxygen Species in Gold Nanoparticle-Targeted Cancer Cells Following Femtosecond Pulse Irradiation. *Sci. Rep.* **2013**, *3*, No. 2146.
(43) Mata, R.; Nakkala, J. R.; Sadras, S. R. Polyphenol Stabilized Colloidal Gold Nanoparticles From *Abutilon indicum* Leaf Extract Induce Apoptosis in HT-29 Colon Cancer Cells. *Colloids Surf., B* **2016**, *143*, 499−510.
(44) Fröhlich, E. The Role of Surface Charge in Cellular Uptake and Cytotoxicity of Medical Nanoparticles. *Int. J. Nanomed.* **2012**, *7*, 5577−5591.
(45) Krishnaraj, C.; Muthukumaran, P.; Ramachandran, R.; Balakumaran, M. D.; Kalaichelvan, P. T. *Acalypha Indica Linn*: Biogenic Synthesis of Silver and Gold Nanoparticles and Their Cytotoxic Effects Against Mda-Mb-231, Human Breast Cancer Cells. *Biotechnol. Rep.* **2014**, *4*, 42−49.
(46) (a) Ramakrishnan, G.; Lo Muzio, L.; Elinos-Báez, C. M.; Jagan, S.; Augustine, T. A.; Kamaraj, S.; Anandakumar, P.; Devaki, T. Silymarin Inhibited Proliferation and Induced Apoptosis in Hepatic Cancer Cells. *Cell Prolif.* **2009**, *42*, 229−240. (b) Kuppusamy, P.; Ichwan, S. J.; Al-Zikri, P. N.; Suriyah, W. H.; Soundharrajan, I.; Govindan, N.; Maniam, G. P.; Yusoff, M. M. In Vitro Anticancer Activity of Au, Ag Nanoparticles Synthesized Using *Commelina nudiflora* L. Aqueous Extract Against HCT-116 Colon Cancer Cells. *Biol. Trace Elem. Res.* **2016**, *173*, 297−305.
(47) Sox, H. C., Jr.; Liang, M. H. The Erythrocyte Sedimentation Rate. Guidelines for Rational Use. *Ann. Intern. Med.* **1986**, *104*, 515−523.
(48) (a) Vedakumari, W. S.; Priya, V. M.; Sastry, T. P. Deposition of Superparamagnetic Nanohydroxyapatite on Iron-Fibrin Substrates: Preparation, Characterization, Cytocompatibility and Bioactivity Studies. *Colloids Surf., B* **2014**, *120*, 208−214. (b) Mohammad, A.; Mehdi, K.; Masoud, K.-S.; Ismaeil, H.; Abbas, B.; Mohammad, A. F.; Shahla, R.; Hamid, A. J.; Fahimeh, S.; Sussan, K. A.; Abbas, S. Evaluation of Multilayer Coated Magnetic Nanoparticles as Biocompatible Curcumin Delivery Platforms for Breast Cancer Treatment. *RSC Adv.* **2015**, *5*, 88096−88107. (c) Shanmugam, R.; Chelladurai, M.; Mahendran, V.; Gurusamy, A. Anticancer and Enhanced Antimicrobial Activity of Biosynthesizd Silver Nanoparticles Against Clinical Pathogens. *J. Mol. Struct.* **2016**, *1116*, 165−173.
(49) Chandra, V. S.; Baskar, G.; Suganthi, R. V.; Elayaraja, K.; Joshy, M. I. A.; Beaula, W. S.; Mythili, R.; Venkatraman, G.; Kalkura, S. N. Blood Compatibility of Iron-Doped Nanosize Hydroxyapatite and Its Drug Release. *ACS Appl. Mater. Interfaces* **2012**, *4*, 1200−1210.
(50) (a) Mohammad, A.; Saeed, B.; Saman, H.; Mohsen, A.; Fahimeh, S.; Abbas, B.; Ismaeil, H. Tuning the Anticancer Activity of a Novel Pro-Apoptotic Peptide Using Gold Nanoparticles Platforms. *Sci. Rep.* **2016**, *6*, No. 31030. (b) Rajeshkumar, S. Anticancer Activity of Eco-Friendly Gold Nanoparticles Against Lung and Liver Cancer. *J. Genet. Eng. Biotechnol.* **2016**, *14*, 195−202.
(51) Masud, R. M.; Biplab, B.; Dibyendu, M.; Dipanwita, M.; Dipak, R.; Sandeep, K. D.; Sourav, C.; Somenath, R.; Joy, S.; Krishnendu, A.; Mukut, C.; Dipankar, C. Anticancer (in vitro) Antimicrobial Effect of Gold Nanoparticles Synthesised Using *Abelmoshus esculentus* (L.) Pulp Extract via Green Route. *RSC Adv.* **2014**, *4*, 37838−37848.
(52) Li, T.; Li, F.; Xiang, W.; Yi, Y.; Chen, Y.; Cheng, L.; Liu, Z.; Xu, H. Selenium-Containing Amphiphiles Reduced and Stabilized Gold Nanoparticles: Kill Cancer Cells via Reactive Oxygen Species. *ACS Appl. Mater. Interfaces* **2016**, *8*, 22106−22112.

DOI: 10.1021/acsomega.7b00353
ACS Omega 2017, 2, 3527−3538